Vol 17 No 9, September 2008
1674-1056/2008/17(09)/3412-05

Chinese Physics B

© 2008 Chin. Phys. Soc.
and IOP Publishing Ltd

Undercooling and solidification of $Ni_{77}P_{23}$ alloy in a 52-m drop tube*

Li Gong(李 工)[a)†], Gao Yun-Peng(高云鹏)[a)], Sun Yi-Nan(孙懿楠)[a)], Chi Zhao-Hong(迟照洪)[b)], and Liu Ri-Ping(刘日平)[a)]

[a)] *Key Laboratory of Metastable Materials Science and Technology, Yanshan University, Qinhuangdao* 066004, *China*

[b)] *National Microgravity Laboratory, Chinese Academy of Sciences, Beijing* 100080, *China*

(Received 11 January 2008; revised manuscript received 21 February 2008)

This paper applies techniques of containerless processing, drop tube and glass fluxing, to undercool and solidify $Ni_{77}P_{23}$ alloys. Different diameter spheres were collected at the bottom of a 52-m long drop tube. Both crystalline and amorphous phase were formed in various size specimens due to the different cooling rate. The variation of partial undercooling with bulk undercooling is calculated for the $Ni_{77}P_{23}$ alloys. The deep undercooling and rapid solidification behaviour of $Ni_{77}P_{23}$ melts has been analysed with respect to microstructure formation and transition during fluxing and 52-m drop process of undercooled melts.

Keywords: crystal morphology, growth models, drop tube
PACC: 6155H, 6150

1. Introduction

The non-equilibrium solidification of liquid metals is attractive in that it produces metastable crystal structure and amorphous phase.[1,2] Rapid solidification and high undercooling techniques are two main ways to realize the solid states far from equilibrium.[3] Containerless[4,5] and glass fluxing[6] methods, for which the nucleation in the melt is almost homogeneous, are widely used to investigate the solidification of undercooled melts. Walker,[7] Schwarz and Herlach[8] found that the phenomenon of grain refinement occurs if the undercooling passes certain critical undercoolings ΔT^*. Samples solidify either into a coarse-grained dendritic microstructure or into a refined equiaxed microstructure.

As a simple binary alloy system, Ni–Cu, Ni–Sn, Ni–S, Ni–P alloys have been widely investigated with several methods, such as drop tube,[4] electromagnetic levitation,[8−10] Pu *et al* [11] researched into the undercooling of bulk melts of $Ni_{81}P_{19}$ eutectic alloys by using fluxing technique and demonstrated that fine cellar eutectic can be obtained for the deep undercooling melt. Up to now, little work focused on dendrite growth kinetics under high undercooling conditions. In this paper, both drop tube and glass fluxing agent techniques were used to obtain high undercooling, the non-equilibrium solidification of the undercooled Ni–P melts was investigated.

2. Experimental procedure

The NiP ingot was first prepared by melting of Ni pieces (purity 99.9%) and Ni_2P powders ((purity 99.8%) under argon atmospheres. The composition was quantified to be $Ni_{77}P_{23}$ by chemical analyses.

As done in Ref.[11], we use B_2O_3 glass to remove the impurity in the NiP ingot. To investigate the influence of cooling rate on amorphous phase formation, a small piece of the NiP sample surrounded by B_2O_3 glass was placed in a quartz tube, which had a small orifice of about 0.3 mm in diameter at the bottom, and then the quartz tube was fixed in the top vacuum chamber of a 52 m-long drop tube. The alloy was remelted by induction heating and further overheated for about 5 min at 1253 K (100 K above its melting point). The temperature is measured by an infrared pyrometer. By blowing with a gas flow of highly purified helium into the quartz tube, the melted sample was ejected out of the nozzle and immediately disintegrated into many droplets. The solidified samples

*Project supported by Hebei province Natural Science Foundation of China (Grant No A200700296), National Natural Science Foundation of China (Grant No 50731005) and National Basic Research Program of China (Grant No 2007CB616915/2006CB605201).
†Corresponding author. E-mail: gongli@ysu.edu.cn

were collected at the bottom of the drop tube.

The experimental set-up of undercooling of NiP alloy in detail can be found in elsewhere.[12] The radiative emission of the droplet is detected along its free-fall path by means of silicon photodiodes located every 5 m along the tube, and recalescence events occurring in an undercooled drop could be detected.

3. Results and discussion

Since the droplet size is directly correlated with the cooling rate during free fall, it was able to determine the cooling rates of melt solidification.[12] The value is 10^3 and 10 K/s corresponding to the samples of 80 and 3000 μm in diameter. For the droplet with about 80 μm in diameter, amorphous phase is obtained.

The x-ray diffraction pattern for the $Ni_{77}P_{23}$ amorphous is shown in Fig.1. A broad peak near 43° followed by another broad peak of lesser intensity is characteristic for the amorphous structure. That is to say, by using a glass encasement technique, where most of the potential sites for heterogeneous nucleation are eliminated, $Ni_{77}P_{23}$ amorphous sphere was formed with a critical cooling rate about 10^3 K/s.

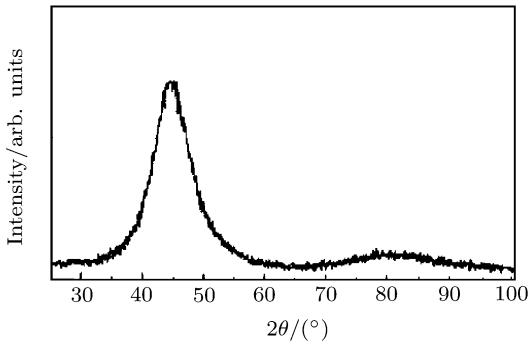


Fig.1. X-ray diffraction pattern for the $Ni_{77}P_{23}$ amorphous alloy with the size of 80 μm in diameter.

In order to investigate the relationship between undercooling and microstructure, we select the solidified balls with the diameter about 3 mm, which correspond to the cooling rate 10 K/s. About 30 NiP samples were processed in the drop tube, while recalescence was detected for 25 samples. The obtained undercooling varied from 20 to 214 K. Figure 2 shows the morphologies

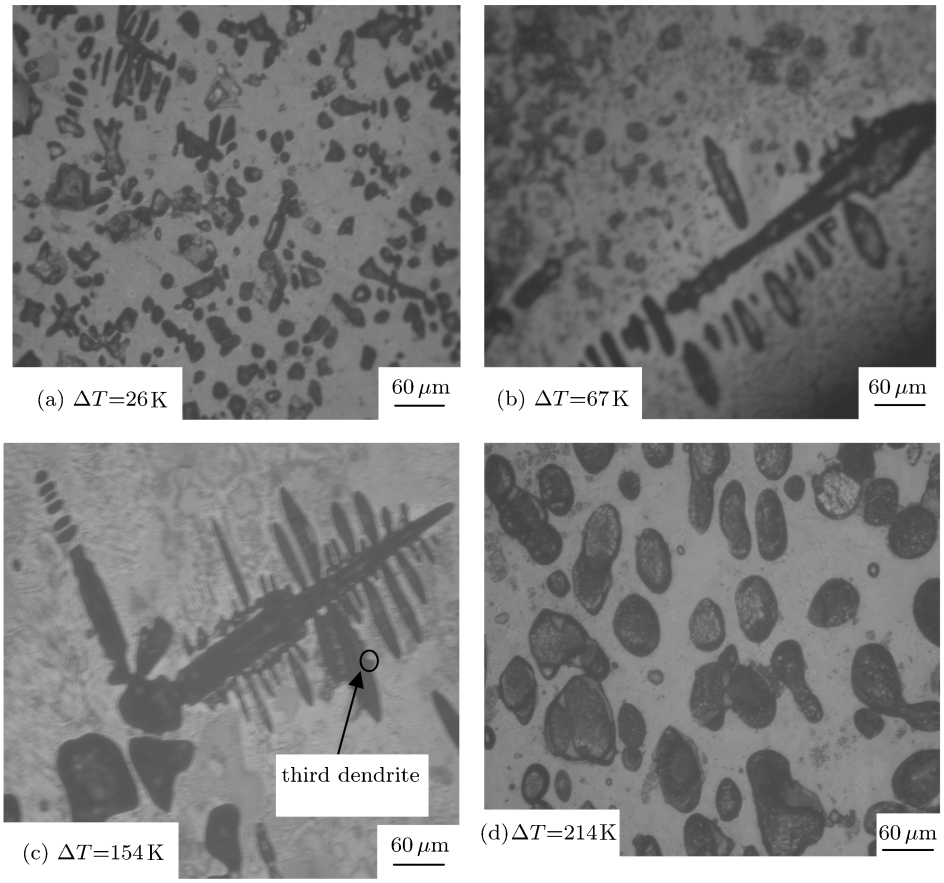


Fig.2. Solidification microstructures of $Ni_{77}P_{23}$ alloy at various undercoolings.

of NiP alloys with different undercooling. Clearly, at small undercooling a refined grain microstructure appears (as shown in Fig.2(a)) which changes at a critical undercooling ΔT_1^* to a coarse-grained dendritic microstructure (see Fig.2(b)). With increasing of the undercooling, the third dendritic microstructure even occurred in Fig.2(c). As shown in Fig.2(d), the grain-refined microstructure re-enters at a critical undercooling ΔT_2^* and prevails at large undercoolings. This double transitional behaviour is also observed in $Ni_{70}Cu_{30}$ alloy.[8] The relationship between the grain morphology and undercooling was listed in Table 1.

Table 1. Relationship between grain morphologies and undercoolings for the NiP samples.

undercooling ΔT/K	30	30–154	154–176	176
microstructure	refined grain	secondary dendrite	third dendrite	refined grain

The phases, at both low (ΔT=26 K) and high undercooling (ΔT=214 K), were identified by x-ray diffraction and shown in Fig.3. Except the x-ray diffraction intensity, the x-ray diffraction patterns of the two solidification microstructures display no trace of any metastable phase other than the Ni and Ni_3P phases, which means that high undercooling only leads to the change of microstructures and does not produce new phase.

It is well known that the phenomenon of grain refinement occurs if the undercooling passes certain critical undercooling ΔT^*. The maximum undercooling of the NiP alloy obtained during experiment is 214 K, which is far beyond the corresponding solidification temperature range and exceeds the critical 0.2 T_l level for homogeneous nucleation predicted by classical nucleation theory.

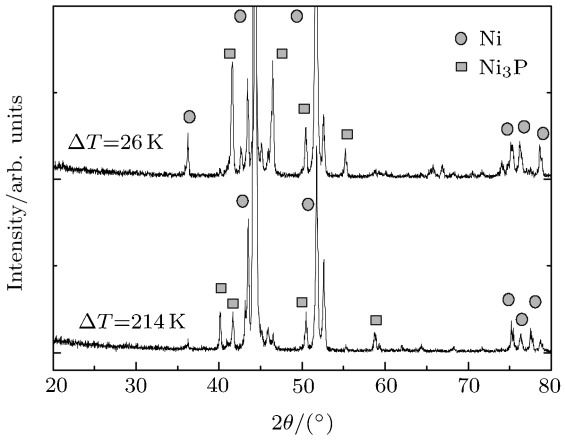


Fig.3. X-ray diffraction patterns of $Ni_{77}P_{23}$ alloy at various undercoolings.

The conditions underlying the solidification of undercooled melts imply dendritic growth which is described in terms of the growth velocity V, undercooling ΔT and the dendrite tip radius r.[13]

The total undercooling is expressed as the sum of four different contributions:[14]

$$\Delta T = \Delta T_t + \Delta T_r + \Delta T_k + \Delta T_c. \tag{1}$$

Here, ΔT_t is the thermal undercooling, ΔT_r the curvature undercooling, ΔT_k the kinetic undercooling, and ΔT_c the solutal undercooling.

$$\Delta T_k = V/\mu, \tag{2}$$

$$\mu = \Delta H_m V_s/(RT_m^2). \tag{3}$$

Here, ΔH_m is the melt heating per unit volume, T_m the melt temperature, R the air constant, V_s the sound velocity in the melt.

$$\Delta T_t = I_v(P_t)\Delta H_m/C_p. \tag{4}$$

Here, P_t=$Vr/(2\alpha_l)$, α_l is the coefficient of thermal diffusion, r the dendrite tip radius, C_p specific heat of melt, V the dendrite growth velocity.

$$I_v(P_t) = P\exp(P)E_1(P), \tag{5}$$

$$E_1 \approx e^{-p}(2p^{\frac{1}{2}} + 3P^{-\frac{5}{2}}), \tag{6}$$

$$\Delta T_r = 2\Gamma/r, \tag{7}$$

$$r = \frac{\Gamma/\sigma^*}{\dfrac{\Delta H_f}{C_p}P_t\xi_t - \dfrac{2m_l'C_0(1-k_v)P_c}{1-(1-k_v)I_v(P_c)}\xi_c}. \tag{8}$$

Here, σ^* is the stable constant, Γ the Gibbs–Thomson coefficient, C_0 the alloy composition, the solutal Peclet number P_c=$Vr/2D$, ξ_t and ξ_c the thermal and solutal stability functions,

$$\xi_t = 1 - \frac{1}{\sqrt{1+\dfrac{1}{\sigma^* P_t^2}}}, \tag{9}$$

$$\xi_c = 1 - \frac{2k_v}{1-2k_v-\sqrt{1+\dfrac{1}{\sigma^* P_c^2}}}. \tag{10}$$

The effective equilibrium liquidus slopes, m_l' and m_l, are calculated as the following expression:

$$m_l' = m_l\left(1 + \frac{k_e - k_v(1-\ln(k_v/k_e))}{1-k_e}\right). \tag{11}$$

The effective solute distribution coefficient:

$$k_{\rm v} = \frac{(k_{\rm e} + \alpha_0 V/D)}{(1 + \alpha_0 V/D)}. \tag{12}$$

Where, α_0 is the characteristic diffusion length, D the diffusion coefficient:

$$D = D_0 \exp\left(- \frac{Q}{RT} \right) \tag{13}$$

and

$$\Delta T_{\rm c} = m_{\rm l} C_0 \left(1 - \frac{m'_{\rm l}/m_{\rm l}}{1 - (1 - k_{\rm v}) I_{\rm v}(P_{\rm c})} \right). \tag{14}$$

Based on the above equations, the calculated results for the undercooling ΔT of NiP alloy are shown in Fig.4, and the physical parameters used during calculation are listed in Table 2. The variation of partial undercooling with bulk undercooling can be found from the curves. The curvature undercooling $\Delta T_{\rm r}$ and kinetic undercooling $\Delta T_{\rm k}$ are less important under the present experimental conditions. While the other two undercooling play different roles within the bulk undercooling. When the undercooling is between 0–80 K, $\Delta T_{\rm c}$ rapidly increases, but the $\Delta T_{\rm r}$ almost does not change until the 90 K, after this point, it increases linearly. At small undercoolings, dendrite growth is controlled mainly by chemical diffusion. As the undercooling further increases, solute trapping sets in, leading to a decrease of the concentration gradient and an increase of the tip radius until the absolute stability of solutal dendrites is reached.[13] When the undercooling is between 30–176 K, there is rather typical dendrite growth. When the bulk undercooling exceeds 176 K (arrow shown in Fig.4), the dominance of $\Delta T_{\rm c}$ will be replaced by the thermal undercooling $\Delta T_{\rm t}$, which means that dendrite growth is purely thermally controlled and the radius begins to fall again due to an increase of the thermal gradient. If the undercooling passes certain higher critical undercooling,[15] due to the rapid release of hearing upon crystallization during the recalesence period, the dendritic arms will break-into and form spheres. This phenomenon was also observed for $Ni_{81}P_{19}$ eutectic alloys.[11]

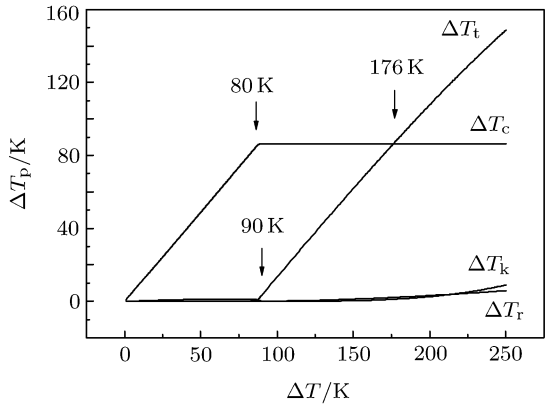


Fig.4. Relationship of partial undercooling versus bulk undercooling.

Table 2. Parameters and values used in the calculations.

parameters	unit	value
$\Delta H_{\rm f}$	J/mol	8.613×10^4
$T_{\rm m}$	K	1.253×10^3
$V_{\rm s}$	m/s	3×10^3
$D_{\rm o}$	m^2/s	1.321×10^{-8}
$D_{\rm l}$	m^2/s	2.61714×10^{-10}
$\alpha_{\rm l}$	m^2/s	10^{-6}
$C_{\rm p}$	J/(K·mol)	0.27×10^3
σ^*	—	$1/4\pi^2$
C_0	—	23
$m_{\rm l}$	K	–23.58
$k_{\rm e}$	—	0.738
R	J/(K·mol)	8.31434
α_0	m	3.24×10^{-10}
Q	J/mol	2.574×10^4
Γ	K·m	1.7×10^{-7}

4. Conclusion

$Ni_{77}P_{23}$ melt was undercooled up to 214 K prior to solidification by combining with drop tube and glass fluxing techniques. Both crystalline and amorphous phase were formed in various size specimens due to the different cooling rates. By eliminating the impurities, NiP amorphous ball formed in a 52-m drop process. The microstructure morphology transition was found when $Ni_{77}P_{23}$ melts exceed a critical undercooling. At small undercoolings a grain refined microstructure appears which changes at a critical undercooling ΔT_1^*=30 K to a coarse-grained dendritic microstructure. The grain-refined microstructure reenters at an upper critical undercooling ΔT_2^*=176 K and prevails at large undercoolings. Once the undercooling exceeds a critical value 176 K, the thermal diffusion will control the dendrite growth.

References

[1] Kui H W, Greer A L and Turnbull D 1984 *Appl. Phys. Lett.* **45** 615

[2] Chen H, Wang W K and Xu Y F 1992 *Acta Phys. Sin.* **41** 1111

[3] Chen L F and Chen X S 1996 *Acta Phys. Sin.* **45** 169

[4] Chen H, Sun G X, Wang W K and Xu Y F 1990 *Acta Phys. Sin.* **39** 836

[5] Cochrane R F, Herlach D M and Feuerbacher B 1991 *Mater. Sci. & Eng.* A **133** 706

[6] Han X J, Yang C, Wei B, Chen M and Guo Z Y 2001 *Mater. Sci. & Eng.* A **307** 35

[7] Walker J L 1959 *The Physical Chemistry of Process Metallurgy* (New York: Interscience) Part 2 p845

[8] Schwarz M, Karma A, Eckler K and Herlach D M 1994 *Phys. Rev. Lett.* **73** 1380

[9] Wei B, Yang G and Zhou Y 1991 *Acta Metall. Mater.* **39** 1774

[10] Leonhardt M, Oeser W and Lindenkreuz H G 1999 *Mater. Sci. & Eng.* A **271** 31

[11] Pu J, Feng W J, Xiao J Z, Gan Z H, Yi H Y and Cui K 2003 *J. Crystal Growth* **256** 139

[12] Li G, Gao Y P, Chi Z H and Liu R P 2007 *J. Alloy and Compound* **433** 233

[13] Herlach D M 1997 *Mater. Sci. & Eng.* A **226–228** 348

[14] Lipton J, Kurz W and Trivedi R 1987 *Acta Metall* **35** 965

[15] Wang C and Wang T M 2003 *Chin. Phys.* **12** 315